

Research Article

NP-MBO: A newton predictor-based momentum observer for interaction force estimation of legged robots

Zhengguo Zhu, Weikai Ding, Weiliang Zhu, Daoling Qin, Teng Chen, Xuewen Rong, Guoteng Zhang*

School of Control Science and Engineering, Shandong University, Jinan 250061, China

ARTICLE INFO

Article history:

Received 17 January 2024

Revised 21 March 2024

Accepted 18 April 2024

Available online 3 May 2024

Keywords:

Interaction force estimation

Momentum-based observer

Newton predictor

Force control

ABSTRACT

Swift perception of interaction forces is a crucial skill required for legged robots to ensure safe human–robot interaction and dynamic contact management. Proprioceptive-based interactive force is widely applied due to its outstanding cross-platform versatility. In this paper, we present a novel interactive force observer, which possesses superior dynamic tracking performance. We propose a dynamic cutoff frequency configuration method to replace the conventional fixed cutoff frequency setting in the traditional momentum-based observer (MBO). This method achieves a balance between rapid tracking and noise suppression. Moreover, to mitigate the phase lag introduced by the low-pass filtering, we cascaded a Newton Predictor (NP) after MBO, which features simple computation and adaptability. The precision analysis of this method has been presented. We conducted extensive experiments on the point-foot biped robot BRAVER to validate the performance of the proposed algorithm in both simulation and physical prototype.

© 2024 The Author(s). Published by Elsevier B.V. on behalf of Shandong University. This is an open access article under the CC BY-NC-ND license (<http://creativecommons.org/licenses/by-nc-nd/4.0/>).

1. Introduction

The capability of real-time interactive force perception is crucial for ensuring the safety, stability, and adaptability of robotic systems across various applications, including manipulation, locomotion, and human–robot interaction [1–3]. Interaction force plays a pivotal role in enabling robots to perceive the characteristics of manipulated objects and interaction surfaces, providing essential references for motion planning [4,5], as shown in Fig. 1. Moreover, interaction force sensing is an essential requirement for implementing disturbance compensation control in robotic systems [6–8]. Some scholars proposed methods for contact estimation and interaction surface perception based on alternative information, such as sound [9,10] and vision [11–13]. However, in dark and noisy environments, force-based tactile sensing provides more stable information for robots during operation.

In recent years, a large number of interactive force estimation methods for robotic systems have emerged. According to their principles of working, they can mainly be categorized into proprioceptive and exteroceptive perception. The exteroceptive perception refers to a category of approaches that require the use of external sensor systems for interaction force estimation. Kim et al. introduced a method to estimate the three-axis contact

force and its position on the cover surface by installing a six-axis force/torque sensor between the cover and the link of the robot manipulator [14]. Long et al. developed an ultra-thin three-axis force sensor for robot wrists based on FBG for real-time interactive force estimation [15]. Dai et al. introduced a flexible and multifunctional intelligent skin for estimating interactive forces and touch positions [16]. While external sensors can yield precise estimation results, the incorporation of additional sensor devices results in heightened system complexity and reduced cross-platform compatibility.

Another category, known as “proprioceptive perception”, relies on utilizing intrinsic information from the robot system, such as joint torques and joint velocities, for the estimation of interaction forces and terrain recognition. This category of methods is widely applied and promoted due to its excellent cross-platform universality. For example, Zhang et al. developed an integral sliding-mode observer to estimate the external forces of Euler–Lagrangian systems [17]. Zhang et al. presented an algorithm for estimating and regulating contact forces in a floating-base system for position control, independent of joint torque information [18]. Apart from this, the momentum-based observer (MBO) [4] is a powerful method for estimating interaction forces, eliminating the need for external sensing devices. This method avoids the use of indirectly measurable joint accelerations by introducing the concept of momentum.

For example, Engelsberger et al. developed an external force estimator based on the MBO concept, enabling the TORO robot to

* Corresponding author.

E-mail address: guoteng@email.sdu.edu.cn (G. Zhang).

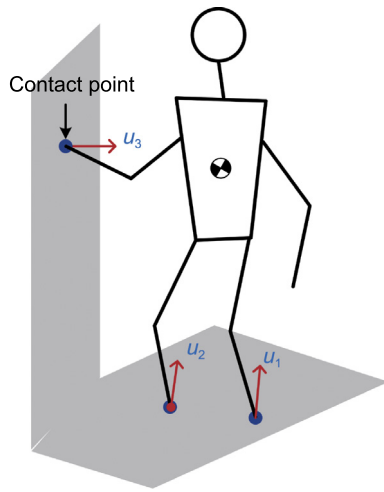


Fig. 1. Diagram illustrating the interaction between the robot and its environment.

withstand external forces equivalent to 15% of its body weight in simulation [19]. Morlando et al. introduced a momentum-based observer, enabling the quadruped robot DogBot to accurately detect external force imposed on the body in simulation [20]. Bretl et al. introduced a discrete-time extension of the generalized momentum disturbance observer for estimating ground reaction forces on the MIT Cheetah 3 robot [21]. However, configuring the cutoff frequency for MBO is a critical issue. A low cutoff frequency can suppress high-frequency noise in estimation results but compromises rapid tracking capability. On the other hand, a high cutoff frequency can accurately capture the contact/release states of the feet but may lead to a decline in estimation accuracy. The rapid tracking capability can provide accurate reference for the robot's contact management, while precise estimation results are a necessary condition for external disturbance compensation. Therefore, striking a balance between the observer's rapid tracking capability and accuracy constitutes a challenge that such observers must confront.

To address this issue, we propose a dynamic cutoff frequency configuration scheme for MBO, aiming to strike a balance between rapidity and accuracy. Furthermore, regardless of the type of filter used in MBO, it inevitably introduces a phase lag in the estimation results. The aforementioned algorithms have scarcely addressed how to cope with the phase lag issue of the observer. Inspired by advancements in radar signal processing [22], we cascaded a Newton predictor (NP) after MBO. This method employs a local modeling approach for extrapolation of the estimated signal to alleviate the phase lag introduced by filtering. We conducted extensive experiments on the torque-controller biped robot BRAVER [23], demonstrating the capabilities of the proposed observer in both simulation and physical prototyping.

The remainder of this paper is organized as follows: In Section 2, we present the dynamic cutoff frequency MBO and its derivation. Section 3 introduces the concept of Newton predictor. Sections 4 and 5 respectively exhibit the experimental results of the simulation and physical prototype.

2. Momentum-based observer

Fig. 2 presents an overview of the observer proposed in this paper. The first part of this algorithm is a MBO derived based on the robot's dynamics model. Differing from conventional algorithms, we implemented a dynamic cutoff frequency configuration scheme for MBO. The second component of the algorithm is

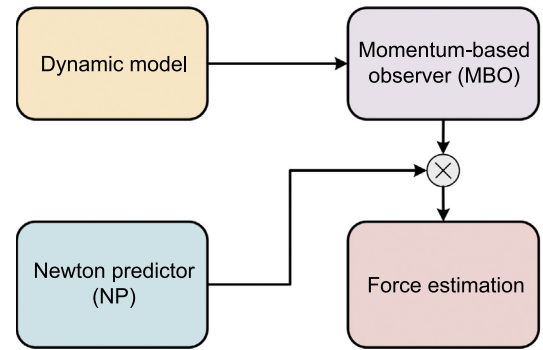


Fig. 2. Overview of the proposed observer.

a Newton predictor, appended after MBO, designed to ameliorate the phase lag introduced by the filter. The derivations provided below are based on a floating base system for illustration, and they are also applicable to systems with a fixed base.

2.1. Robot dynamics

As the robot maneuvers through the environment, its resultant dynamic model can be formulated as

$$\mathbf{M}(\mathbf{q})\ddot{\mathbf{q}} + \mathbf{C}(\mathbf{q}, \dot{\mathbf{q}})\dot{\mathbf{q}} + \mathbf{g} = \mathbf{S}^T \boldsymbol{\tau} + \sum_{i \in \mathcal{C}} \mathbf{J}_i^T(\mathbf{q})\mathbf{u}_i \quad (1)$$

where $\mathbf{M} \in \mathbb{R}^{(6+n) \times (6+n)}$, $\mathbf{C} \in \mathbb{R}^{(6+n) \times (6+n)}$, $\mathbf{g} \in \mathbb{R}^{6+n}$ are the inertia matrix, Coriolis matrix and gravity vector, respectively; $\mathbf{S} = [\mathbf{0}_{n \times 6} \quad \mathbf{I}_n]$ is the actuated part selection matrix; $\boldsymbol{\tau} \in \mathbb{R}^n$ is the actuation torques; $\mathbf{u}_i \in \mathbb{R}^{3n_c}$ is the ground reaction forces (GRFs) of i th supporting limb; $\mathbf{J}_i \in \mathbb{R}^{3n_c \times (6+n)}$ represents the Jacobians that transpose the GRFs into the acceleration of the COM and the actuated joints for the i th contact limb, while n and n_c denote the number of active degrees of freedom (DoF) and the number of limbs in the support state, respectively. The set \mathcal{C} contains all subscripts corresponding to limbs in contact.

2.2. Interaction force estimation

The proprioceptive-based interaction force estimation method was firstly proposed in [4] for manipulator collision sensing. This approach avoids reliance on force sensing devices and angular acceleration signals that are not directly measurable. The effectiveness of this method has been validated on multiple platforms [7, 24]. Therefore, we still base our interactive force observer design on this concept.

By isolating the joint motion component from Eq. (1), we can derive

$$\mathbf{S}_j (\mathbf{M}(\mathbf{q})\ddot{\mathbf{q}} + \mathbf{C}(\mathbf{q}, \dot{\mathbf{q}})\dot{\mathbf{q}} + \mathbf{g}) = \boldsymbol{\tau} + \mathbf{S}_j \sum_{i \in \mathcal{C}} \mathbf{J}_i^T(\mathbf{q})\mathbf{u}_i \quad (2)$$

here, $\mathbf{S}_j \in \mathbb{R}^{n \times (n+6)}$ represents the selection matrix for the components of the limbs. Consider the force transmitted by each contact point as an external disturbance, and define a vector to represent it

$$\boldsymbol{\tau}_d = \mathbf{S}_j \sum_{i \in \mathcal{C}} \mathbf{J}_i^T(\mathbf{q})\mathbf{u}_i \quad (3)$$

To mitigate the impact of high-frequency noise, a filtered variant of this vector, denoted as $\hat{\boldsymbol{\tau}}_d$, can be computed in the following manner:

$$\hat{\boldsymbol{\tau}}_d = \mathbf{G}_F(z)\boldsymbol{\tau}_d \quad (4)$$

where z denotes the z -domain variable, and Δt signifies the sampling period; and $G_F(z)$ is a discrete filter and its i th diagonal element takes the following form

$$G_{F,i}(z) = \frac{b_0 + b_1 z^{-1} + b_2 z^{-2} + \dots + b_m z^{-m}}{a_0 + a_1 z^{-1} + a_2 z^{-2} + \dots + a_n z^{-d}} \quad (5)$$

where, m represents the degree of the numerator polynomial, while d indicates the degree of the denominator polynomial.

Bledt et al. [21] configured $G_{F,i}$ in the form of a first-order low-pass filter and proposed an alternate derivation of this observer fully in discrete time, rendering the model more faithful to the actual situation. This approach computes the acceleration term $M\ddot{\mathbf{q}}$ through a convolution sum, utilizing the discrete-time equivalent of integration by parts referred to as summation by parts. Due to the superior filtering performance and response speed of a second-order filter compared to a first-order low-pass filter [25], in this paper, we use a discrete MBO augmented with a second-order low-pass filter

$$G_{F,i}(z) = \frac{(1 - \lambda_{1,i})}{1 - \lambda_{1,i} z^{-1}} - \frac{(1 - \lambda_{2,i})}{1 - \lambda_{2,i} z^{-1}} \quad (6)$$

where $\lambda_{1,i}$ and $\lambda_{2,i}$ are filter coefficients. Then, $G_F(z)M(\mathbf{q})\ddot{\mathbf{q}}$ can be written as

$$G_F(z)M(\mathbf{q})\ddot{\mathbf{q}} = \sum_{k=0}^N w_{n-k} M(\mathbf{q}_k) \ddot{\mathbf{q}}_k \quad (7)$$

where w_k represents the impulse response of the filter. Learned from [21], Eq. (7) can be transformed into the following form

$$B\rho_{n+1} - \sum_{k=0}^n w_{n-k} \left(\frac{1}{\Delta t} (M_{k+1} - M_k) \dot{\mathbf{q}}_{k+1} + B\rho_{k+1} \right) \quad (8)$$

where B is a diagonal gain matrix, and its i th diagonal element is

$$B_i = \beta_{1,i} - \beta_{2,i}, \quad \beta_{j,i} = (1 - \lambda_{j,i}) \lambda_{j,i}^{-1} / \Delta t, \quad j = 1, 2 \quad (9)$$

where $\rho = M\dot{\mathbf{q}}$ is the generalized momentum. Then, by using the forward Euler method

$$\frac{1}{\Delta t} (M_{k+1} - M_k) = \dot{M}_k \quad (10)$$

and the property of the inertia matrix M [26]

$$\dot{M} = C + C^T \quad (11)$$

Eq. (7) can be simplified as

$$G_F(z)M\ddot{\mathbf{q}} = B\rho - G_F(z)(C\dot{\mathbf{q}} + C^T\dot{\mathbf{q}} + B\rho) \quad (12)$$

Assuming $\rho(0) = \mathbf{0}$ indicates that the observer's initialization must precede the robot control. Consequently, Eq. (4) can be reformulated as

$$\hat{\tau}_d = BS_j\rho - G_F(z)S_j(B\rho + S^T\tau + C^T\dot{\mathbf{q}} - \mathbf{g}) \quad (13)$$

Subsequently, the interaction force for each leg can be obtained by

$$\mathbf{u}_i = (S_i J_i^T)^{-1} S_i \hat{\tau}_d \quad (14)$$

where S_i denotes the selector matrix for the joints in limb i , J_i represents the Jacobian matrix for the i th supporting leg, and \mathbf{u}_i stands for the GRFs of the i th supporting leg.

2.3. Dynamic cutoff frequency

Let λ be the cutoff frequency of the second-order low-pass filter in Eq. (6), and T be the gait cycle. For legged robots, the GRFs is one of the crucial indicators for assessing contact status. Therefore, we anticipate that the estimated GRFs by the

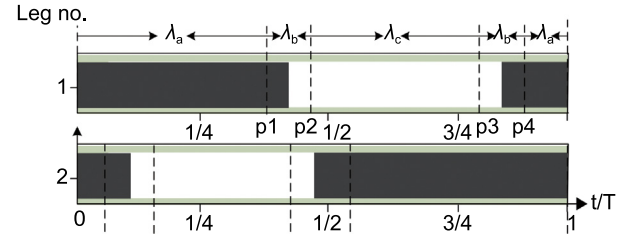


Fig. 3. Dynamic cutoff frequency diagram. In this case, using a bipedal robot as an example, 1 and 2 denote the left and right legs. The dark areas indicate the support phase, while the white areas indicate the swing phase.

observer should promptly reflect the transition process between support and swing phases. However, this presents a contradictory choice—setting the cutoff frequency too high enhances the observer's rapid tracking ability but results in the estimation incorporating a significant amount of noise, especially when in the swing phase. Conversely, setting it too low leads to a degradation in tracking performance. In our case, we implemented a dynamic frequency configuration method. When in the vicinity of the transition phase between support and swing, the cutoff frequency is increased to swiftly capture the contact/swing states. When the phase is far from the transition states, the cutoff frequency is reduced to obtain accurate estimation results. In our case, we employ the dynamic cutoff frequency configuration method as illustrated in Fig. 3, with its mathematical expression given as follows:

$$\lambda = \begin{cases} \lambda_a, & 0 \leq t/T \leq p1, \\ \lambda_b, & p1 \leq t/T \leq p2 \\ \lambda_c, & p2 \leq t/T \leq p3 \\ \lambda_b, & p3 \leq t/T \leq p4 \\ \lambda_a, & p4 \leq t/T \leq 1 \end{cases} \quad (15)$$

3. Newton predictor

The above derivation reveals that, inevitably, filters are employed in the MBO. The filter is capable of efficiently filtering noise; however, it may induce phase lag, which poses a significant disadvantage for high real-time control systems. Given that the robot systems primarily depend on state feedback control, excessively delayed feedback information may lead to oscillations and even instability of the system. A major solution to resolving this issue is to model the estimated signal. The NP exhibit a desirable trait for extrapolation of polynomials, owing to their inherent attributes of having a straightforward design process and a relatively low computational complexity [27]. In our work, the NP is utilized to alleviate the phase lag of the estimated acceleration signals. In this article, we present only a subset of important equations and their derivations. For more detailed information, please refer to [28].

3.1. Principle of Newton predictor

For a set of $M+1$ distinct real numbers x_0, x_1, \dots, x_M with corresponding values y_0, y_1, \dots, y_M , there exists a unique polynomial p_M of degree at most M that fulfills the following condition:

$$\begin{bmatrix} 1 & x_0 & x_0^2 & \dots & x_0^M \\ 1 & x_1 & x_1^2 & \dots & x_1^M \\ 1 & x_2 & x_2^2 & \dots & x_2^M \\ \vdots & \vdots & \vdots & \vdots & \vdots \\ 1 & x_M & x_M^2 & \dots & x_M^M \end{bmatrix} \begin{bmatrix} v_0 \\ v_1 \\ v_2 \\ \vdots \\ v_M \end{bmatrix} = \begin{bmatrix} y_0 \\ y_1 \\ y_2 \\ \vdots \\ y_M \end{bmatrix} \quad (16)$$

where $v_i, i \in [0, M]$ represents a constant representing the coefficients of the polynomial.

To write the above equation in polynomial form, we have

$$p_M(x) = \sum_{j=0}^M c_j \prod_{i=0}^{j-1} (x - x_i) \quad (17)$$

with

$$c_j = \frac{y_j - p_{j-1}(x_j)}{(x_j - x_0)(x_j - x_1) \dots (x_j - x_{j-1})}, \quad p_0 \equiv c_0 = y_0 \quad (18)$$

It can be expressed in polynomial form as follows:

$$p_M(x) = \zeta_1 + \zeta_2 x + \zeta_3 x^2 + \dots + \zeta_M x^{M-1} + \zeta_{M+1} x^M \quad (19)$$

where the polynomial coefficients $\zeta_j, j \in [0, M]$, are unknown real constant. M is the order of the assumed polynomial. As per [27], the N -step ahead NP for an M -order polynomial can be represented by a z -domain transfer function:

$$H_M^N(z) = \sum_{k=0}^M (1 - z^{-N})^k \quad (20)$$

where N is the prediction horizon. The above equation demonstrates that the NP possesses the advantage of a reduced computational load, rendering it particularly suitable for implementation in the onboard controllers of legged robots characterized by limited computing resources. Moreover, during practical computations, it is not necessary to know the coefficients of the polynomial, so in a sense, it can also be considered as an adaptive estimator. Substituting Eq. (20) into Eq. (13) and extrapolating for $\hat{\tau}_d$ yields:

$$\tilde{\tau}_d = H_M^N(z) \hat{\tau}_d \quad (21)$$

Subsequently, we substitute $\tilde{\tau}_d$ into Eq. (14) to solve for interaction forces. Eq. (20) indicates that the newton predictor requires two parameters, n and M , to be predefined by the user. Increasing M will improve the degree of approximation between the polynomial and the actual signal, but it requires the utilization of information from more past moments. Excessively utilizing past estimated values for forward prediction can result in error accumulation, ultimately leading to a reduction in the precision of the estimation. Increasing N will result in longer predictions of the estimated signal, but it will also increase estimation errors. The selection of these two values needs to be based on the actual circumstances. In practical deployment, the smaller the passband of the low-pass filter, the more pronounced the effect of the predictor will be.

3.2. Precision analysis

In this section, we will elaborate on the quantitative analysis using polynomial approximation of acceleration signals. As discussed in [29], low-order polynomials can provide accurate approximations for many real-world signals.

Assuming $p(x)$ is a polynomial of degree at most M which interpolates $f(x)$ at the $M + 1$ distinct points x_0, x_1, \dots, x_M in $[a, b]$, that is

$$p_M(x) = \sum_{j=0}^M c_j \prod_{i=0}^{j-1} (x - x_i) \quad (22)$$

with

$$p_M(x_i) = f(x_i), \quad i = 0, 1, \dots, M \quad (23)$$

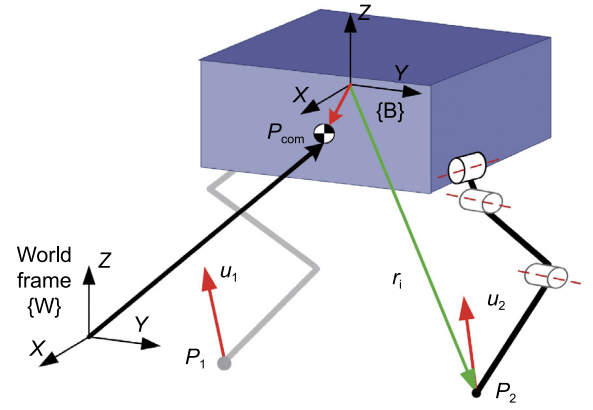


Fig. 4. The topological diagram and coordinate system definition of BRAVER. W is the world coordinate system and B is the body attached frame.

As analyzed in [28], if the M th-order derivatives of $f(x)$ exist for each $x \in [a, b]$ there exists a number $\xi_x \in (a, b)$ such that

$$f(x) - p(x) = \frac{1}{(M+1)!} f^{(M+1)}(\xi_x) \prod_{i=0}^M (x - x_i) \quad (24)$$

where $f \in C^{M+1}[a, b]$, $(M+1)! = (M+1)(M)(M-1) \dots 2 \cdot 1$. Define Δx_i as the distance between the i th data point and the $(i-1)$ th data point, we have

$$\Delta x_i = x_i - x_{i-1} \quad (25)$$

In real-time robotic systems, the sampling points are equally spaced, thus

$$\Delta t = \Delta x_i \quad (26)$$

According to Eq. (26), the following inequality holds

$$\prod_{i=0}^M |x - x_i| \leq \frac{1}{4} \Delta t^{M+1} M! \quad (27)$$

If we also assume that the derivatives of $f(x)$ are bounded, i.e., $|f^{(M+1)}(x)| \leq \hbar$, then we get

$$|f(x) - p(x)| \leq \frac{\hbar}{4(M+1)} \Delta t^{M+1} \quad (28)$$

Thus, the error for interpolation with degree- M polynomials is $\mathcal{O}(\Delta t^{M+1})$. When deployed on legged robots, a limited number of historical moments is usually chosen, and M is not large, making the above assumption feasible.

4. Simulations

To gauge the algorithm's performance, we conducted multiple sets of experiments within a simulated environment. The NP-MBO described in this article is evaluated on our virtual robot, called "BRAVER", illustrated in Fig. 4. Both the locomotion control loops and interactive forces estimator are executed in real-time threads operating at a frequency of 500 Hz. The robot was set up to execute high-dynamic walking with a stepping frequency of 2.5 Hz and a gait duty cycle of 0.55. In all comparative experiments, MBO and NP-MBO were configured with the same cutoff frequency. Due to the lower noise level in the simulation environment, a consistent cutoff frequency is applied throughout the entire phase. Throughout all tests, we employed $M = 2$ and $N = 1$ in the Newton Predictor for forward prediction.

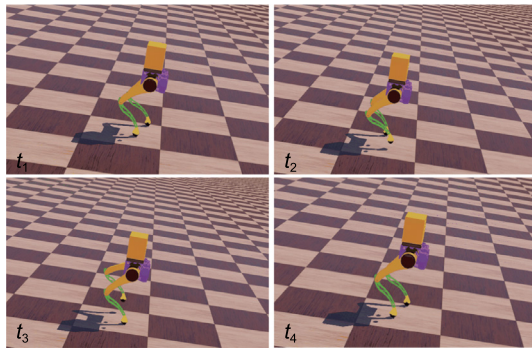


Fig. 5. A sequential snapshot of the simulation scenario for the GRFs estimation experiment.

Table 1 Comparison of RSME under different estimation schemes.

Case	RSME	
	NP-MBO	MBO
GRFs(x)	3.9418	4.5359
GRFs(y)	3.9721	6.8936
GRFs(z)	3.499	18.4357

4.1. Real-time GRFs estimation

A key aspect of the observer presented in this article is its utilization of the Newton Predictor, which enhances the phase lag of force estimation outcomes. To demonstrate its effectiveness, we conducted comparative experiments between using MBO and NP-MBO. In this test, we use two observers to estimate the real-time interaction forces during robot walking and compare them with the true values. The snapshots of this experiment is shown in Fig. 5.

The performance of these two approaches is qualitatively assessed by determining which one yields a lower Root Mean Squared Error (RMSE). Fig. 6 shows the experimental data indicates that the presented method exhibits a superior ability to rapidly track real-time interaction forces in comparison to the traditional MBO. The RMSE data shown in Table 1 further validates the conclusion that the proposed algorithm can enhance the estimation accuracy compared to the traditional MBO.

4.2. External disturbance estimation

To further demonstrate the performance of our observer, we conducted a comparative test for external disturbance perception. The simulation is configured to have BRAVER walk at a constant speed in the +x direction. Subsequently, a disturbance with a maximum force of 10 N is applied to the robot’s center of mass in the y direction. Simultaneously, we utilized the external force estimation scheme proposed in [8] to estimate the disturbance. The locomotion controller, gait timing, and external disturbance remain consistent across both tests, with the only difference being the interactive forces estimation scheme. Fig. 7 illustrates a sequential series of snapshots depicting the simulated scenario for this experiment. Fig. 8 presents estimated data for the GRFs during dynamic locomotion. It demonstrates that our proposed approach improves the accuracy of disturbance force estimation compared to the traditional MBO. It is worth noting that the lag in disturbance estimation observed in Fig. 8 stems from the particular filtering structure of the algorithm in [8], and is not caused by the observer proposed in this paper.

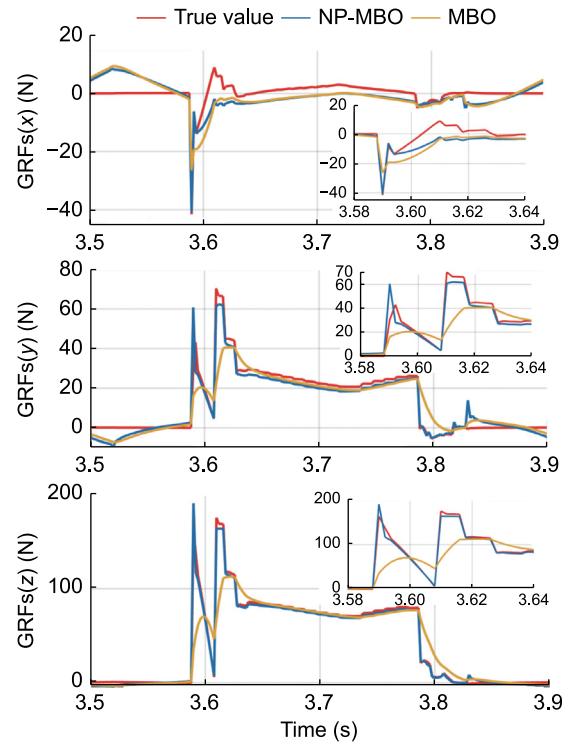


Fig. 6. Simulation. Comparison of ground reaction forces estimation for different observers. GRFs(x), GRFs(y) and GRFs(z) represent the plantar forces in the x, y and z directions respectively.

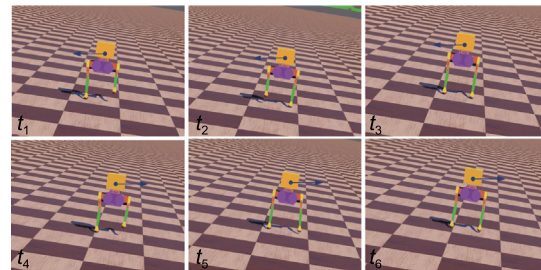


Fig. 7. Snapshots of disturbance estimation. The blue arrows represent external disturbances.

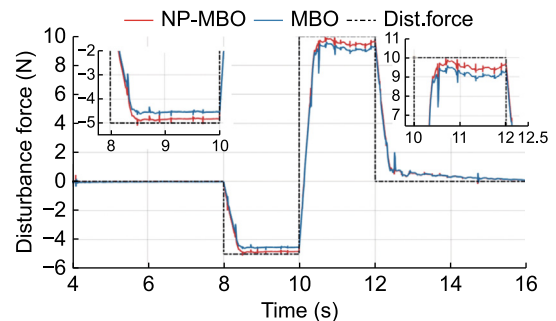


Fig. 8. Simulation. Comparison of external disturbances estimation for different interaction force observers.

5. Experiment

5.1. Comparison of GRFs estimation

To evaluate the practical applicability of the proposed algorithm in real-world scenarios, we conducted experimental

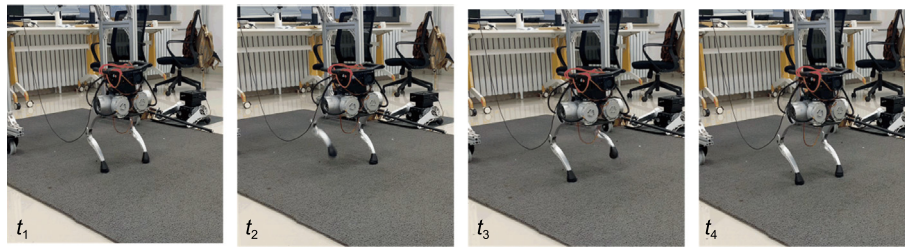


Fig. 9. Snapshots of real-time GRFs estimation.

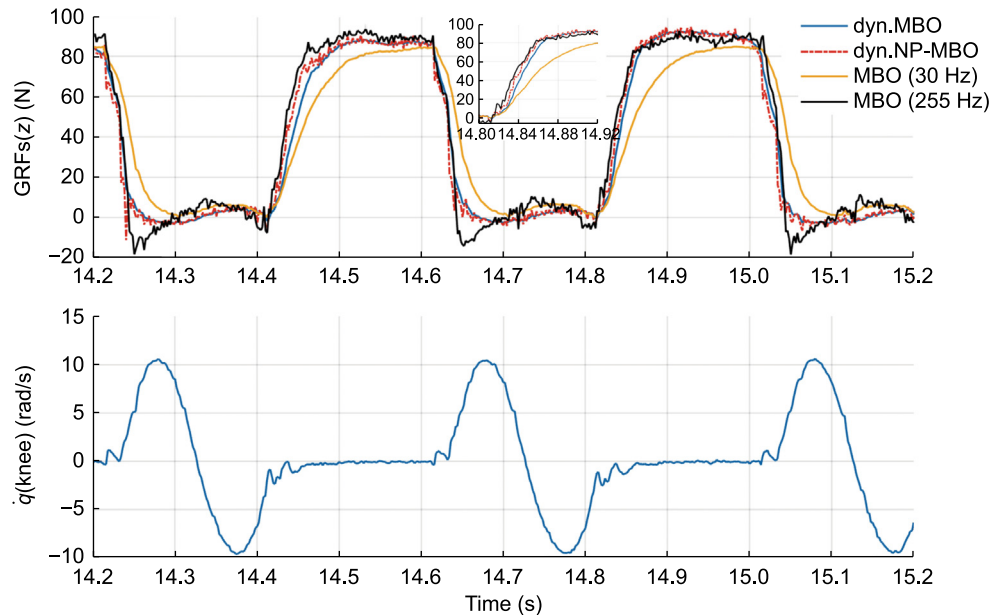


Fig. 10. Comparison of interaction force estimation for different schemes during bipedal robot walking. All data is extracted from the right leg.

validation using the point-footed biped robot BRAVER. The prototype experiments maintained the same stepping frequency and gait duty factor as employed in the simulations. We conducted four sets of comparative experiments, including fixed-frequency MBO (with cutoff frequencies of 255 Hz and 30 Hz), dynamic-frequency MBO (dyn. MBO), and dynamic-frequency NP-MBO (dyn. NP-MBO). In this test, the dynamic frequencies λ_a , λ_b , and λ_c were set to 70 Hz, 255 Hz, and 30 Hz, respectively. We utilized the four distinct observers for the estimation of GRFs during the dynamic walking of the biped robot. Figs. 9 and 10 exhibit the snapshots and estimation results of this experiment, respectively. The MBO with a cutoff frequency of 255 Hz exhibits good rapidity; however, there are noticeable numerical fluctuations, and significant deviations in estimation results occur when the legs are in the swing phase. The MBO with a cutoff frequency of 30 Hz exhibits significant phase lag. On the contrary, dynamic cutoff frequency MBO achieves a certain degree of balance between rapidity and accuracy. NP-MBO can further enhance the lag induced by the filter, especially during contact state transitions.

5.2. Load perception

To validate the performance of the proposed algorithm in practical application scenarios, we also conducted experiment on BRAVER interaction force estimation under load conditions. In this experiment, we placed a box weighing approximately 1 kg on the head of the robot while it was walking, and then instructed the robot to move while carrying the box. The snapshot of the experimental process is shown in Fig. 11. During this process, we

utilized the proposed interaction force observer to estimate the variation of the robot's plantar force. Upon the addition of a load, the robot necessitates increased force to maintain its stability, leading to pronounced changes in its plantar force. This experiment seeks to ascertain whether our algorithm can accurately perceive changes in interaction forces during this process. The experimental results, as shown in Fig. 12, demonstrate that our proposed observer can sensitively capture changes in interaction forces resulting from variations in the robot's load. Moreover, the change in the vertical plantar force is approximately equal to the gravitational force of the box placed on the robot's head (approximately 10 N).

6. Conclusion

In this paper, we propose a novel proprioceptive-based interactive force observer. Firstly, it replaces the conventional fixed cutoff frequency setting in the traditional MBO with a dynamic cutoff frequency configuration, aiming to strike a balance between rapidity and accuracy. Secondly, compared to previous algorithms, we take into account the phase lag in the estimation results caused by filters in the MBO. Motivated by signal processing work in radar and related fields, we incorporated a newton Predictor after MBO, modeling the estimated signal near the update point as a polynomial and employing this polynomial for forward prediction to improve phase lag. We validated the efficacy of the proposed observer through simulations and physical tests conducted on the biped robot BRAVER.

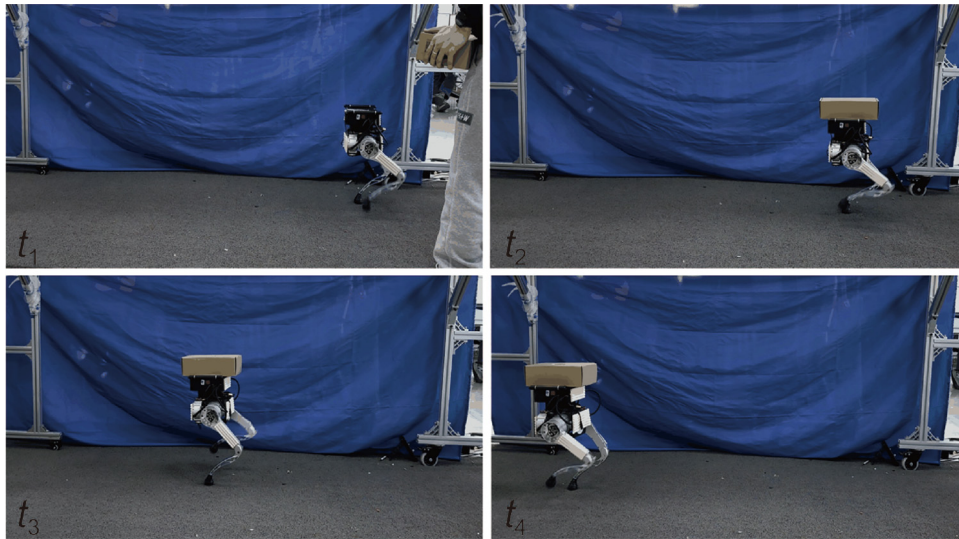


Fig. 11. Snapshots of bipedal robot BRAVER walking with external load.

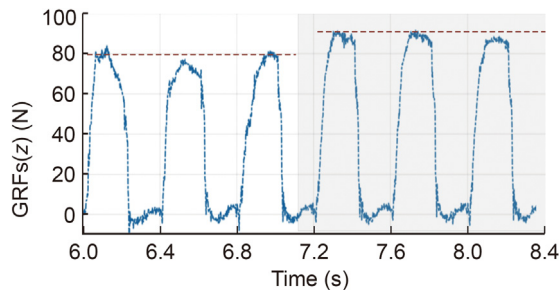


Fig. 12. GRFs data of bipedal robot BRAVER during walking.

In future work, we will validate the accuracy and speed of interaction force estimation on robotic arm systems or humanoid robots. Additionally, developing a contact detection algorithm for legged robots based on this algorithm is also one of the future tasks.

CRediT authorship contribution statement

Zhengguo Zhu: Data curation, Formal analysis, Methodology, Validation, Writing – original draft. **Weikai Ding:** Data curation, Formal analysis, Validation. **Weiliang Zhu:** Validation. **Daoling Qin:** Validation. **Teng Chen:** Project administration, Writing – review & editing. **Xuewen Rong:** Funding acquisition, Project administration. **Guoteng Zhang:** Funding acquisition, Project administration, Supervision, Validation.

Declaration of competing interest

The authors declare that they have no known competing financial interests or personal relationships that could have appeared to influence the work reported in this paper.

Acknowledgments

This work was supported in part by the National Key Research and Development Program of China (2022YFB4701504), the National Natural Science Foundation of China (62373223 and 62203268), and Youth Innovation and Technology Support Plan for Higher Education Institutions in Shandong Province (2023KJ029).

Appendix A. Supplementary data

Supplementary material related to this article can be found online at <https://doi.org/10.1016/j.birob.2024.100160>.

References

- [1] A. Dietrich, C. Ott, Hierarchical impedance-based tracking control of kinematically redundant robots, *IEEE Trans. Robot.* 36 (1) (2020) 204–221.
- [2] X. Bao, S. Guo, Y. Guo, C. Yang, L. Shi, Y. Li, Y. Jiang, Multilevel operation strategy of a vascular interventional robot system for surgical safety in teleoperation, *IEEE Trans. Robot.* 38 (4) (2022) 2238–2250.
- [3] J. Heinzmann, A. Zelinsky, Quantitative safety guarantees for physical human-robot interaction, *Int. J. Robot. Res.* 22 (7–8) (2003) 479–504.
- [4] A. De Luca, A. Albu-Schaffer, S. Haddadin, G. Hirzinger, Collision detection and safe reaction with the DLR-iii lightweight manipulator arm, in: 2006 IEEE/RSJ International Conference on Intelligent Robots and Systems, 2006, pp. 1623–1630.
- [5] M. Camurri, M. Fallon, S. Bazeille, A. Radulescu, V. Barasuol, D.G. Caldwell, C. Semini, Probabilistic contact estimation and impact detection for state estimation of quadruped robots, *IEEE Robot. Autom. Lett.* 2 (2) (2017) 1023–1030.
- [6] F. Jenelten, R. Grandia, F. Farshidian, M. Hutter, TAMOLS: Terrain-aware motion optimization for legged systems, *IEEE Trans. Robot.* 38 (6) (2022) 3395–3413.
- [7] M. Focchi, R. Orsolino, M. Camurri, V. Barasuol, C. Mastalli, D. Caldwell, C. Semini, Heuristic planning for rough terrain locomotion in presence of external disturbances and variable perception quality, 2018.
- [8] Z. Zhu, G. Zhang, Z. Sun, T. Chen, X. Rong, A. Xie, Y. Li, Proprioceptive-based whole-body disturbance rejection control for dynamic motions in legged robots, *IEEE Robot. Autom. Lett.* 8 (11) (2023) 7703–7710.
- [9] D. Qin, G. Zhang, Z. Zhu, X. Zeng, J. Cao, An online terrain classification framework for legged robots based on acoustic signals, *Biomim. Intell. Robotics* 3 (2) (2023) 100091, [Online]. Available: <https://www.sciencedirect.com/science/article/pii/S2667379723000050>.
- [10] J. Christie, N. Kottege, Acoustics based terrain classification for legged robots, in: 2016 IEEE International Conference on Robotics and Automation, ICRA, 2016, pp. 3596–3603.
- [11] M.M. Venâncio, R.S. Gonçalves, R.A.d.C. Bianchi, Terrain identification for humanoid robots applying convolutional neural networks, *IEEE/ASME Trans. Mechatronics* 26 (3) (2021) 1433–1444.
- [12] P. Filitchkin, K. Byl, Feature-based terrain classification for LittleDog, in: 2012 IEEE/RSJ International Conference on Intelligent Robots and Systems, 2012, pp. 1387–1392.
- [13] F. Yang, C. Chen, Z. Wang, H. Chen, Y. Liu, G. Li, X. Wu, Vit-based terrain recognition system for wearable soft exosuit, *Biomim. Intell. Robotics* 3 (1) (2023) 100087, [Online]. Available: <https://www.sciencedirect.com/science/article/pii/S2667379723000013>.
- [14] U. Kim, G. Jo, H. Jeong, C.H. Park, J.-S. Koh, D.I. Park, H. Do, T. Choi, H.-S. Kim, C. Park, A novel intrinsic force sensing method for robot manipulators during human-robot interaction, *IEEE Trans. Robot.* 37 (6) (2021) 2218–2225.

- [15] J. Long, Q. Liang, W. Sun, Y. Wang, D. Zhang, Ultrathin three-axis FBG wrist force sensor for collaborative robots, *IEEE Trans. Instrum. Meas.* 70 (2021) 1–15.
- [16] Y. Dai, S. Gao, A flexible multi-functional smart skin for force, touch position, proximity, and humidity sensing for humanoid robots, *IEEE Sens. J.* 21 (23) (2021) 26355–26363.
- [17] Z. Zhang, M. Leibold, D. Wollherr, Integral sliding-mode observer-based disturbance estimation for Euler–Lagrangian systems, *IEEE Trans. Control Syst. Technol.* 28 (6) (2020) 2377–2389.
- [18] G. Zhang, S. Ma, Y. Li, Contact force estimation and regulation of a position-controlled floating base system without joint torque information, in: 2020 IEEE/RSJ International Conference on Intelligent Robots and Systems, IROS, 2020, pp. 3967–3974.
- [19] J. Engelsberger, Combining Reduced Dynamics Models and Whole-Body Control for Agile Humanoid Locomotion (Ph.D. dissertation), 2016.
- [20] V. Morlando, A. Teimoorzadeh, F. Ruggiero, Whole-body control with disturbance rejection through a momentum-based observer for quadruped robots, *Mech. Mach. Theory* 164 (2021) 104412.
- [21] G. Bledt, P.M. Wensing, S. Ingersoll, S. Kim, Contact model fusion for event-based locomotion in unstructured terrains, in: 2018 IEEE International Conference on Robotics and Automation, ICRA, 2018, pp. 4399–4406.
- [22] J. Bingbing, L. Qian, Y. Kun, D. Qianli, M. Xianchao, H. Fei, D. Ke, A RLSN-based current statistical model for target range tracking, in: 2021 CIE International Conference on Radar (Radar), 2021, pp. 902–906.
- [23] Z. Zhu, W. Zhu, G. Zhang, T. Chen, Y. Li, X. Rong, R. Song, D. Qin, Q. Hua, S. Ma, Design and control of BRAVER: a bipedal robot actuated via proprioceptive electric motors, *Auton. Robots* (2023) 1–15.
- [24] F. Jenelten, R. Grandia, F. Farshidian, M. Hutter, TAMOLS: Terrain-aware motion optimization for legged systems, *IEEE Trans. Robot.* 38 (6) (2022) 3395–3413.
- [25] V. Morlando, A. Teimoorzadeh, F. Ruggiero, Whole-body control with disturbance rejection through a momentum-based observer for quadruped robots, *Mech. Mach. Theory* 164 (2021) 104412, [Online]. Available: <https://www.sciencedirect.com/science/article/pii/S0094114X21001701>.
- [26] B. Siciliano, L. Sciacvico, L. Villani, G. Oriolo, *Robotics: Modelling, Planning and Control*, first ed., Springer Publishing Company, Incorporated, 2008.
- [27] S. Ovaska, O. Vainio, Recursive linear smoothed Newton predictors for polynomial extrapolation, *IEEE Trans. Instrum. Meas.* 41 (4) (1992) 510–516.
- [28] P.J. Davis, *Interpolation and Approximation*, Courier Corporation, 1975.
- [29] W. Feller, *An Introduction to Probability Theory and its Applications*, John Wiley & Sons, 2008.